FISEVIER

Contents lists available at ScienceDirect

Materials Characterization

journal homepage: www.elsevier.com/locate/matchar



Pre-compression effect on microstructure evolution of extruded pure polycrystalline magnesium during reversed tension load



Duke Culbertson^a, Qin Yu^{a,1}, Jian Wang^b, Yanyao Jiang^{a,*}

- ^a University of Nevada, Reno, Department of Mechanical Engineering, Reno, NV 89557, USA
- ^b University of Nebraska-Lincoln, Department of Mechanical and Materials Engineering, Lincoln, NE 68588, USA

ARTICLE INFO

Keywords: Magnesium Twinning Detwinning Pre-compression Reversed tension

ABSTRACT

The microstructure evolution of extruded pure polycrystalline magnesium under compression followed by subsequent tension in ambient air was investigated. Solid round dog-bone shaped specimens were compressed along the extrusion direction (ED) to -7.3% and -12.8% true strains, respectively, and then tensioned along the ED to failure. Electron backscatter diffraction (EBSD) was used to examine the microstructure evolution using companion specimens unloaded at multiple points along the deformation curves. Pre-compression along the ED resulted in $\{10\bar{1}2\}$ tension twinning which increased in volume with increasing strain until exhaustion at approximately -10.5% true strain. Tensile reloading of the pre-compressed specimens led to a combination of low Schmid factor twinning, detwinning, and secondary $\{10\bar{1}2\}$ tension twinning. Detwinning was more significant than secondary twinning in the -7.3% pre-compressed specimens, where only one secondary twin variant was observed. $\{10\bar{1}2\}$ secondary twinning was more significant in the -12.8% pre-compressed specimens, where up to three secondary twin variants were observed. After complete detwinning of primary twins, the secondary twins were retained and appeared as sub-grains. The residual sub-grains resulted from secondary twinning may provide a strengthening mechanism for wrought Mg alloys.

1. Introduction

Magnesium (Mg) and its alloys are attractive materials for structural components due to their excellent physical properties such as low density, high specific strength, and good machinability. Mg plastically deforms via slips and twinning due to its hexagonal close-packed (HCP) crystal structure. $\{10\overline{1}2\}$ tension twinning is one major twinning deformation mode because of the low critical resolved shear stress, and it mainly accommodates the deformation along the c-direction of the hexagonal lattice [1–3]. Apart from the commonly observed tension twins, there is $\{10\overline{1}1\}$ compression twinning [4–6]. During mechanical loading, multiple twins can be activated and interact with each other, resulting in a compression-tension double twin [7–10], tension-tension double twin (or secondary tension twin) [11–14], or tension-compression-tension tertiary twin [15,16]. The resulting microstructure due to twinning further changes the mechanical properties of Mg and Mg alloys.

A strong basal texture is usually formed in Mg alloys after the rolling and extrusion manufacturing processes. Twinning can significantly change the initial texture of the wrought Mg alloys and will consequently affect the deformation and fracture of the material. Under monotonic loading [17–27], cyclic loading [28–36], and loading path change conditions [37–40], crystal reorientation caused by tension twinning allows for easier activation of the (0001) basal slip. Therefore, altering the initial texture and microstructure through pre-deformation could lead to optimized mechanical properties of as-wrought Mg alloys. For instance, tension-compression anisotropy of as-wrought Mg alloys can be reduced through mitigation of the initial basal texture driven by pre-compression along the extruded direction (ED) or rolled direction (RD) [41]. Likewise, compressive yield strength can be enhanced by inducing twin boundaries as grains are refined through pre-compression [42].

Pre-deformation experiments can be classified into two categories. The first type of experiments involves two-step (or multi-step) monotonic compression [41–48]. Initial twins are introduced in the material through pre-compression along the ED or RD. Re-compression is applied along the same ED or RD, or along the orthotropic transverse direction (TD) [42,44,46]. It is found that re-compression, applied either in the same direction or in the orthotropic direction, leads to an increase in the compressive yield strength [41–48]. The strengthening mechanism during re-compression in the same direction is ascribed to the texture change and the decreased twinning capacity [42], whereas

^{*} Corresponding author.

E-mail address: yjiang@unr.edu (Y. Jiang).

¹ Current address: Schlumberger-Doll Research Center, One Hampshire St, Cambridge, MA 02139.

during re-compression in the orthotropic direction, the increased resistance to detwinning contributes to the yield strengthening [44]. In the microscopic aspect, detwinning can be observed during the recompression along the orthotropic direction. In addition to detwinning, double tension-tension twinning was identified after re-compression [42–44,48]. The activation of double tension-tension twins was attributed to the observed enhancement of the ultimate strength during recompression [42–44].

For the second type of pre-deformation experiments, alternation of loading direction in the consecutive multi-step deformation is engaged [49–53]. Following a loading step with tension (or compression), compression (or tension) loading is applied in the pre-tension (or precompression) deformed samples. This pre-deformation scenario provides a practical means to design complex twin structure for material strengthening and toughening. Song et al. [48] showed that pre-tension along the RD can modify the initial basal texture where the $\langle 10\bar{1}0 \rangle$ poles are concentrated towards the RD. Such a texture tuning fosters the activation of multiple twin variants when compression is applied subsequently along the TD. As multiple twin variants induce twin boundaries and twin-twin interactions, the grain-refinement hardening effect is enhanced.

Compared to the extensive work on the microstructure evolution in the two-step (multi-step) compression experiments, there are limited studies carried out to investigate the pre-compression effect on deformation and microstructure change during subsequent reversed tension [49–53]. It is noticed that the pre-compressive strain in most of the prior studies was < 8%. No studies have been carried out to study the effects of large pre-compression on reversed tensile deformation. The current work aims at studying the effect of pre-compression (both small and large strain) on the subsequent tensile deformation in extruded polycrystalline pure Mg. In particular, the microstructure evolution will be examined in the companion specimens using electron backscatter diffraction (EBSD) characterization. Important twinning modes and their roles on deformation will be identified.

2. Material and Experiments

Solid round dog-bone shaped specimens, as shown in Fig. 1a, were cut from an extruded pure polycrystalline Mg rod. The specimen had a gage length of 12.7 mm and a diameter of 10.0 mm in the gage section. Fig. 1b, an inverse pole figure (IPF) map according to EBSD analysis, shows initial microstructure of the extruded pure polycrystalline Mg. The material is composed of untwinned and equiaxed grains with an average size of $100~\mu m$. The pole figure (PF) (Fig. 1c) suggests that the material has a strong a-axis texture, where the c-axes are aligned along the radial direction and perpendicular to the ED of the extruded bar. Prior to mechanical testing, the specimen surface was polished to 600/P1200 grit.

Mechanical experiments were conducted using an Instron 8500 load

frame in ambient air. A strain rate of $4.5 \times 10^{-3} \, \mathrm{s}^{-1}$ was used for both tension and compression loading. In addition to monotonic tension and monotonic compression experiments, companion specimens were used to study the pre-compression effect on the subsequent microstructure evolution. The true stress-strain responses for different loading paths are shown in Fig. 2. Five specimens were compressed to true strains of -0.7%, -3.0%, -7.3%, -10.5%, and -12.8%, respectively, for the study of twin nucleation and growth during monotonic compression. Three specimens were pre-compressed to -7.3% followed by reversed tension to -4.1%, 2.0%, and tension failure (4.8%), respectively. Companion specimens for the -12.8% pre-strain path were unloaded at -9.4%, -2.0%, and 4.3% (failure) strain under the subsequent tensile loading. True stress and true strain are reported and will be used henceforth.

Following the mechanical experiments, cylindrical samples with a thickness of 3 mm were sectioned in the middle of the gage section perpendicular to the loading axis or ED (refer to Fig. 1a) for EBSD observations. For the fractured specimens, the EBSD samples were sectioned away from the fracture surface but still within the gage section. The sample surface was ground, polished, and etched. Grinding was done sequentially using silicon carbide grit paper from 320/P400 grit to 600/P1200 grit, and then polished using 6 μm and 1 μm oil based polycrystalline diamond suspension. Final polish was achieved using 0.05 μm alumina-based suspension. The samples were etched in a Picral-Acetic solution of 10 mL glacial acetic acid, 4.2 g picric acid, 10 mL distilled water, and 70 mL 200 proof ethanol. For each companion specimen, two EBSD scans of 1200 $\mu m \times 1000$ μm area with a step size ranging from 0.35 to 0.6 μm were performed.

To facilitate a discussion of twins, labeling will be used according to Ref. [42], in which " T_i " indicates the twin variant. "T" is used to describe tension twin while subscript "i" specifies twin variant. The tension $\{10\bar{1}2\}$ $\langle\bar{1}011\rangle$ twin has six crystallographic equivalent variants due to the symmetry of the HCP crystal. T_1 corresponds to the $\{10\bar{1}2\}$ $[\bar{1}011]$ variant, while increasing subscripts correspond to the other variants by counter-clockwise rotation about the c-axis. Double tension twins or a secondary tension twin formed within a primary twin will be denoted according to Ref. [13]. For example, " T_{ij} " denotes a " T_{j} " secondary twin formed within a " T_{i} " primary twin.

3. Results and Discussions

3.1. Microstructure Evolution during Compressive Pre-Deformation

The microstructure and texture of the extruded pure polycrystalline Mg under monotonic compression at -3.0%, -7.3%, and -12.8% strain are shown in Fig. 3. At a strain of -3.0%, the IPF map reveals clearly identifiable twin bands. Among the 209 grains within the observation area, 160 grains (76.6%) contain at least one tension twin variant and 85 grains (40.7%) contain two or more twin variants. The

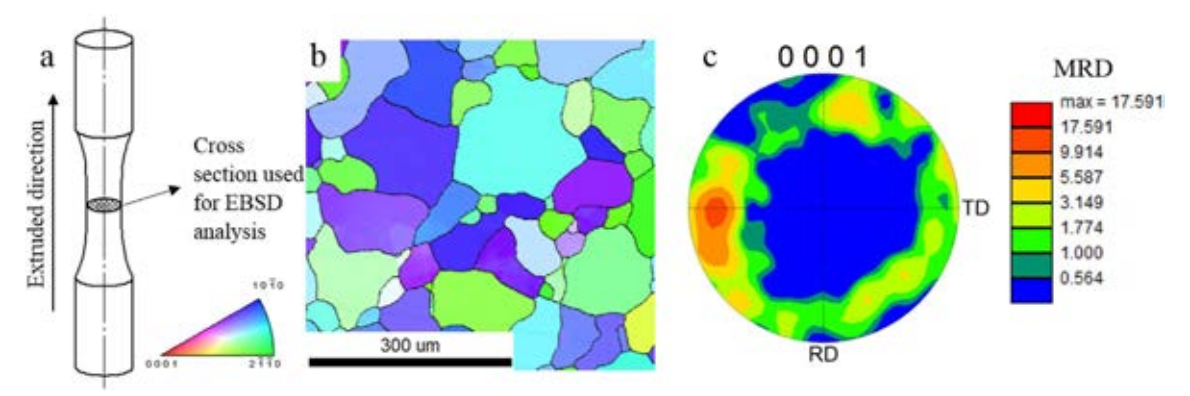


Fig. 1. (a) Solid cylindrical dog-bone specimen of extruded pure polycrystalline magnesium, (b) initial inverse pole figure map, and (c) pole figure.

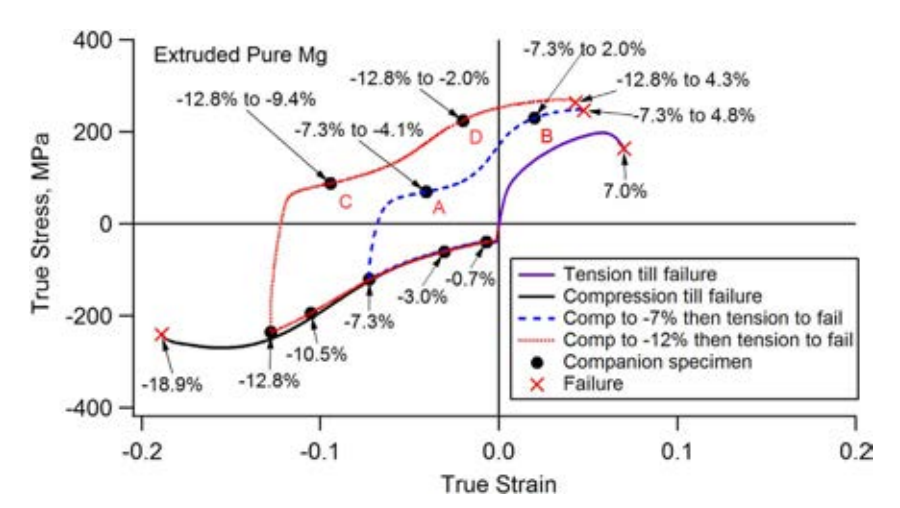


Fig. 2. Loading paths and corresponding companion specimens, indicated by markers along the loading curves, examined at each loading condition.

twin volume fraction (TVF) is 12.4%. Twinning at this stage predominantly follows the Schmid factor (SF) criterion with respect to the original orientation of parent grains.

Early studies [7,22,40] suggest that the SFs of the six tension twin variants under compression perpendicular to the c-axis differ from those under tension along the c-axis. Assuming an ideal crystal orientation, compression along the $\langle 10\overline{1}0 \rangle$ direction will results in one cozone variant pair with a large SF of 0.499 and two pairs with a low SF of 0.1247. Alternatively, compression along the $\langle 2\overline{1}10 \rangle$ direction (a-axis) results in two co-zone variant pairs with an SF of 0.374 and the remaining variant pair with an SF of zero. For the compression direction between $\{10\overline{1}0\}$ and $\langle 2\overline{1}10\rangle$, one co-zone variant pair will have the largest SFs. This is consistent with the findings in the -3.0% strain IPF map where 62 grains (accounting for 72.9% of the 85 grains with two or more twin variants) contain co-zone twin pairs.

Twinning during compressive pre-strain results in a rotation of c-axis away from the radial direction in the extruded cylindrical bar towards the extrusion direction. The overall texture evolution is visualized in the progression of (0001) pole figures from Fig. 3a–c where the peak intensity values of the multiples of random density (MRD) move from the edge of the figure towards the center. This texture evolution is reflected in the IPF maps. One to two variants, often a co-zone variant pair, are commonly identified in close to prismatic $\{10\overline{10}\}$ orientated grains ("blue grains") in Fig. 3a. Alternatively, two to four variants, or up to two sets of co-zone variant pairs, are commonly identified in grains close to an a-axis $\{2\overline{110}\}$ orientated grain ("green grains"). Co-zone variant pairs rotate about the same axis, only in opposite directions, so they share a small theoretical misorientation angle of 7.4° and have similar SF values. As a result, co-zone twin variants are difficult to differentiate in the IPF maps.

With increasing compressive strain, nucleation of more twins and the growth and coalescence of twins result in an increase in twin volume fraction. When the compressive strain reaches -7.3%, the twinned area accounts for 69.9% of the scanned area. This increase in TVF is reflected in the pole figure where there is a higher (0001) density towards the center of the figure than towards its edge, unlike what is seen for -3.0% strain. Fig. 3b reveals that the twins activated at - 3.0% strain have grown and the coalescence of twins has been initiated. Co-zone variant pairs appear to coalesce together, as seen in Fig. 3d, where the co-zone pair variants are both identified uniquely, as well as within a coalesced twin region. A misorientation analysis on these co-zone variant pairs, using "average grain orientations," yields a misorientation angle of 4° to 6° between the two variants, which is lower than the theoretical misorientation angle of 7.4°. In nearly a-axis {2110} orientated grains, adjacent twin variants collide and result in some unusual twin morphology.

At a strain of -12.8% strain, twinning is exhausted and the TVF

reaches 93.7% as most of the grains are fully twinned. However, the orientation varies spatially in a grain and is associated with low angle boundaries (< 7°) that are ascribed to coalescence of co-zone variant pair similar to what was observed at -7.3% strain in Fig. 3b. Additionally, the co-zone variant pairs often surround any additional twin variants activated, resulting in the appearance of sub-grains, as observed in Fig. 3c and d. The sub-grains formed tend to deviate from the often-found lenticular shape of tension twinning, with curved or wavy boundaries. Both of these observations are likely the result of the interaction of twin dislocations at the boundary of the variants involved [42]. An example of these observations can be seen in Fig. 3e where a nearly *a*-axis grain forms two primary twin variants under compression. However, one variant, "variant 1," has the largest SF and dominates most of the original grain and may also be the coalescence of a co-zone variant pair. "Variant 2" is an adjacent twin to "variant 1," and has a smaller SF value than the more significant "variant 1." A misorientation analysis of these two variants yields a misorientation of approximately 55° between them, which is 5° less than the theoretical value of 60°. It is interesting to note that the IPF color of both variants is similar and would be difficult to differentiate without highlighting the boundaries.

3.2. Tension after a Pre-compressive True Strain of -7.3%

A tension load after a pre-compression strain of -7.3% results in detwinning and secondary twinning because of thicker twins and twintwin interactions generated by a pre-compression strain of -7.3%. Results shown in Fig. 4a and b, corresponding to strain ranges of 3.2% and 12.1%, respectively, from the pre-compression state, reveal that the applied tensile load leads predominantly to detwinning where the originally twinned areas are isolated from other twin variants and twinned back to the original parent orientation. In addition to detwinning, two other twinning phenomena are observed. The first is the formation of low or negative SF twins, which are often found in unfavorable twinning grains under pure tension [54,55]. The second twinning phenomenon, as presented in Fig. 4c, is the formation of secondary tension twins within the primary twins that were produced during pre-compression. Such a phenomenon is usually observed in grains that have an original prismatic {1010} parent orientation, and may be a result of its ideal orientation for activating a single set of co-zone variant twin pairs. Based on the SF values previously discussed for an ideal crystal, the nearly prismatic $\{10\overline{1}0\}$ grains have a larger SF value for twin variants than the nearly a-axis $\{2\overline{11}0\}$ grains. Therefore, it is speculated that primary twinning is easier to activate in these nearly $\{10\overline{1}0\}$ grains and consequently, twinning exhaustion may occur under less strain than the nearly {2110} grains. Additionally, the primary twin from the prismatic $\{10\overline{1}0\}$ grain, such as that shown in Fig. 4b, has its *c*-axis almost perfectly aligned with the loading axis. Upon reversed tension, this orientation is

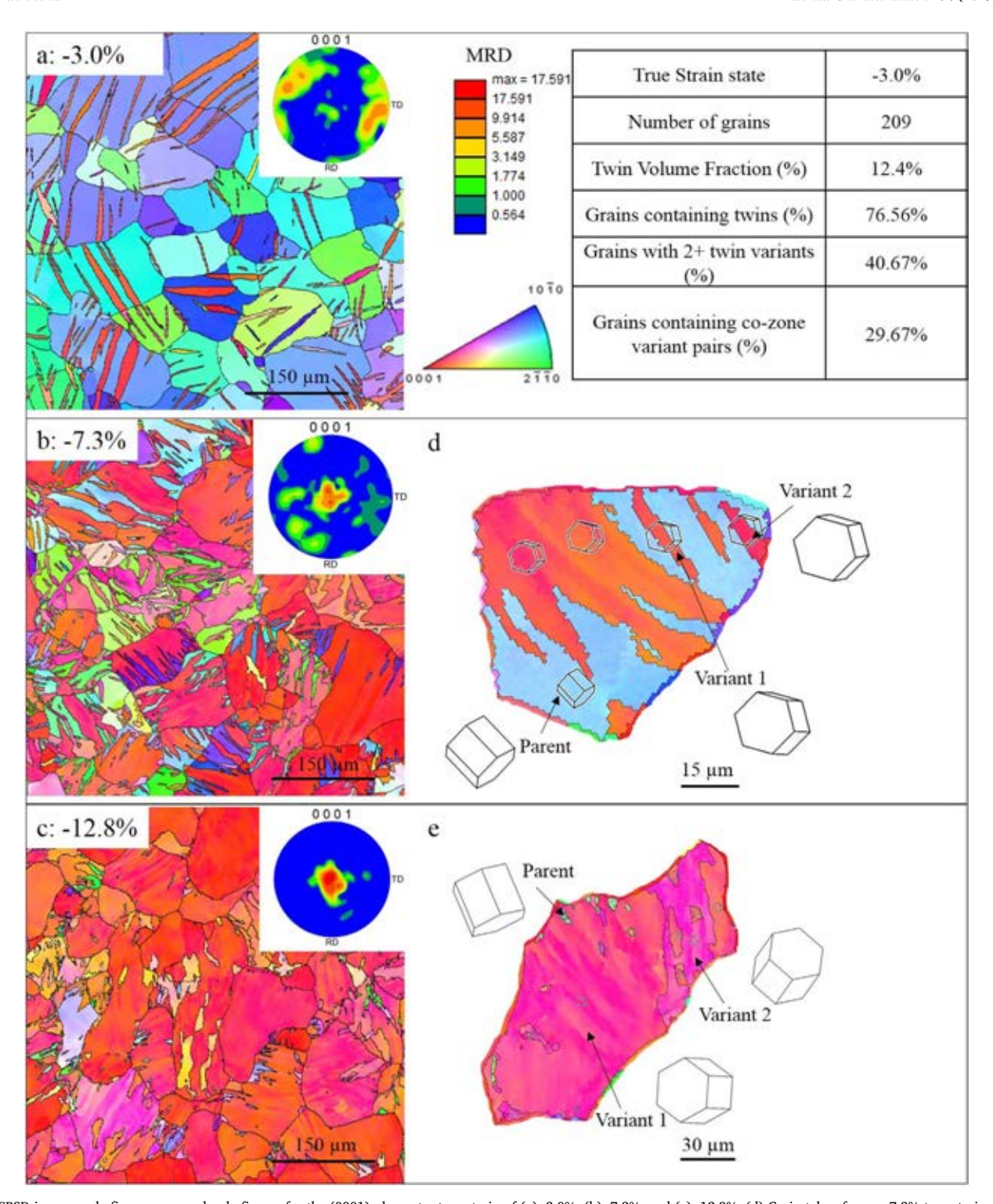


Fig. 3. EBSD inverse pole figure maps and pole figures for the (0001) plane at a true strain of (a) -3.0%, (b) -7.3%, and (c) -12.8%. (d) Grain taken from -7.3% true strain showing coalescence of a co-zone variant pair. (e) Grain taken from -12.8% true strain showing two primary twin variants of different orientations but similar IPF color.

more favorable for secondary tension twinning than those primary twins formed in the a-axis $\{2\overline{11}0\}$ grains.

Fig. 4c and d reveal two cases of secondary twinning and detwinning as a result of re-tension from the -7.3% pre-strain. The presented parent unit cells show very strong prismatic $\{10\overline{1}0\}$ orientations in which the c-axis is nearly perpendicular to the loading direction. Under compression, the grain is easily twinned to the primary twin variant T_1 as shown in Fig. 4c. The presented parent unit cell in Fig. 4d would also have been twinned under compression. However, there are no residual

primary twin areas remaining following the tension to failure. It is expected that these grains would have been almost completely twinned at a -7.3% compressive strain. At point 'A' in the loading curves of Fig. 2, secondary tension twinning is observed concurrently with detwinning. Only one secondary twin variant is activated despite its favorable orientation for tension twinning. The misorientation between the secondary twin variant and the parent is identified by an axis angle pair of approximately 60° about [10 $\overline{10}$]. Additionally, given the amount of detwinning that has occurred, it appears that detwinning is more

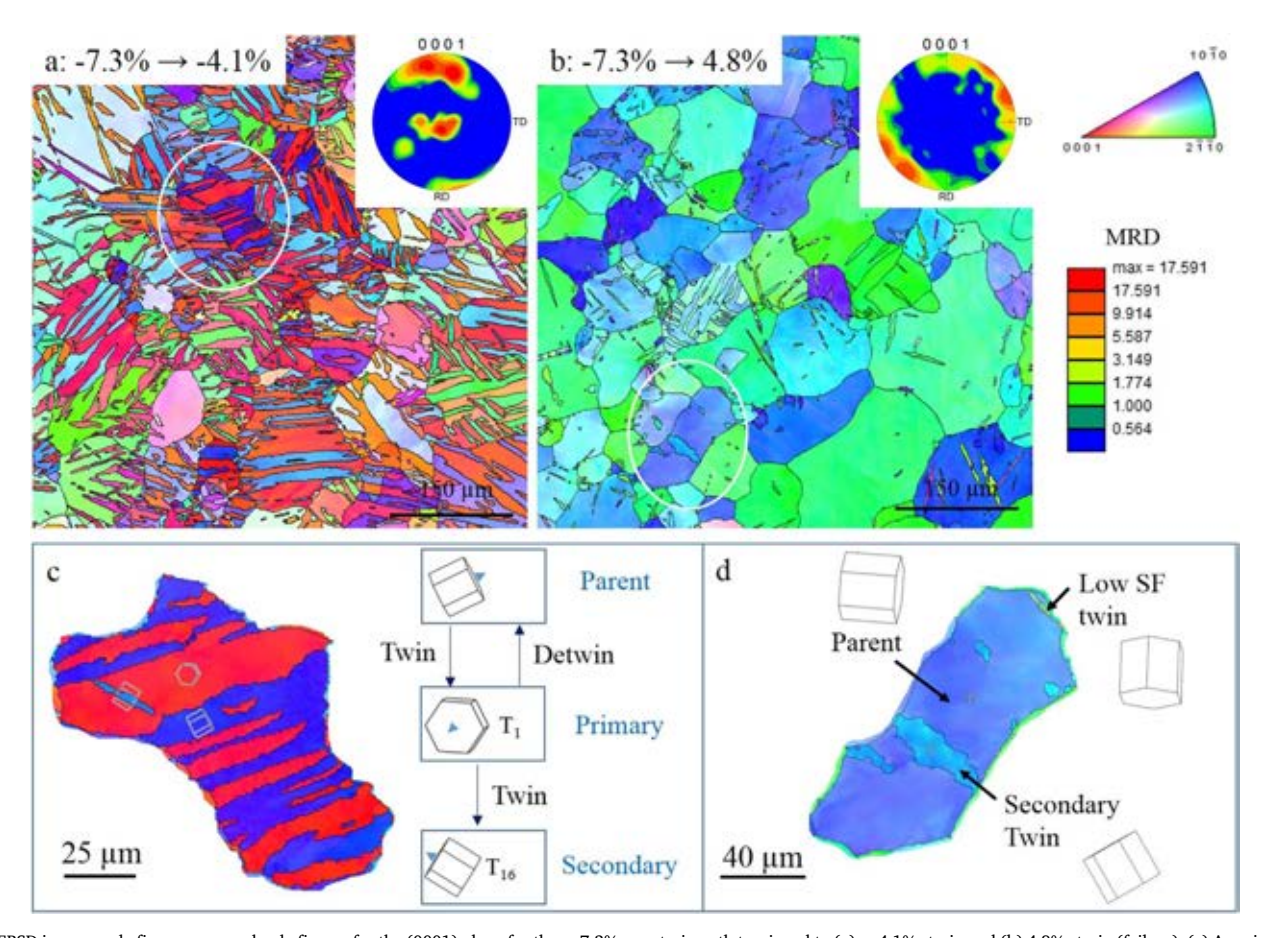


Fig. 4. EBSD inverse pole figure maps and pole figures for the (0001) plane for the -7.3% pre-strain path tensioned to (a) -4.1% strain and (b) 4.8% strain (failure). (c) A grain marked in (a) depicting both detwinning and secondary twinning as a result of the reversed tensile loading. Arrows in the hexagonal unit cell depict the c-axis. " T_i " signifies tension twin and the subscript "i" specifies the variant. " T_{ij} " denote a " T_j " secondary twin forming inside a " T_i " primary twin. (d) A grain marked in Fig. 4b displaying sub-grains formed from secondary tension twinning and the low SF twins. (For interpretation of the references to color in this figure legend, the reader is referred to the web version of this article.)

favorable than the formation of additional secondary twinning. This is consistent with the study of twin-twin interaction in Mg [13].

When detwinning, which may or may not include the formation of the new secondary twins, is exhausted by point B in the loading curves in Fig. 2, the overall microstructure and texture at point B in Fig. 2 are similar to those at tensile failure from the same pre-strain. At failure under tension, detwinning is complete, revealing a mostly original texture but with scattered low SF twins and sub-grains. Fig. 4d is taken from the specimen that experienced -7.3% pre-strain followed by tension to failure. Two regions are characterized with nearly prismatic orientation. A misorientation analysis of the two regions reveals an axis-angle misorientation of 60° about [1010], similar to the misorientation observed in Fig. 4c. Further analysis indicated that the small-sized sub-grain is a secondary tension twin formed during the reversed tension. These secondary twins are of various shapes and sizes, ranging from the lenticular shape commonly associated with tension twins to small irregular-shaped fragments surrounded by the nearly original oriented parent. It is speculated that these small secondary twin sub-grain fragments are nucleated in the primary twins and grow during the reversed tension while the primary twins are fully detwinned. Apart from the sub-grains formed during secondary twinning, there is a low SF twin in narrow width, originating from the dominant prismatic area, present locally in the upper right corner of the grain (Fig. 4d). Such a low SF twin is likely due to the local stresses at/near grain boundary [54,55].

3.3. Tension after a Pre-compressive True Strain of -12.8%

A pre-strain to -12.8% results in minor differences from those of

the -7.3% pre-compression strain in influencing the evolution of microstructure and texture during the subsequent tensile loading (Fig. 5a and b). A careful examination of the microstructure in Fig. 5c (corresponding to point C in Fig. 2) reveals that more than one secondary twin variant can be activated in the previously twinned regions. Fig. 5c highlights a grain from Fig. 5a that contains multiple secondary twin variants. Compression from a speculated parent orientation results in two primary twin variants, T_1 and T_2 , where the dominant variant is T_2 . The subsequent tensile load activates up to three secondary twin variants T₁, T₄, and T₅ within the dominant primary variant T₂, that are labeled by T21, T24 and T25. T25 variant is the co-zone variant pair to the parent (which is fully detwinned and correspondingly can be labeled by T22). In addition, T25 variant could be the co-zone variant pair to the T₁₂ variant that is formed in the primary twin T₁. This secondary twinning phenomenon, while similar in procedure to what is seen in Fig. 4 for the -7.3% pre-strain, appears to have a more significant impact on the microstructure and texture shown in Fig. 5. The increase of pre-strain increases the amount of secondary twin variants, which is accompanied by an increase in the overall volume consumed by the secondary twins. The increase of the number of secondary twins and the area consumed by secondary twinning results in an increase of subgrains when the primary twin is fully detwinned. Fig. 5d shows a grain that contains 14 sub-grains that have two secondary twin variants within a parent orientation. Comparing Fig. 5b with Fig. 4b, it is observed that the volume of sub-grains increases with the increased prestrain value. More variants or sub-grains formed in the larger pre-strain specimen result in a more randomized a-axis texture as shown by the pole figure in Fig. 5b, and significantly contribute to the grain-refinement hardening effect.

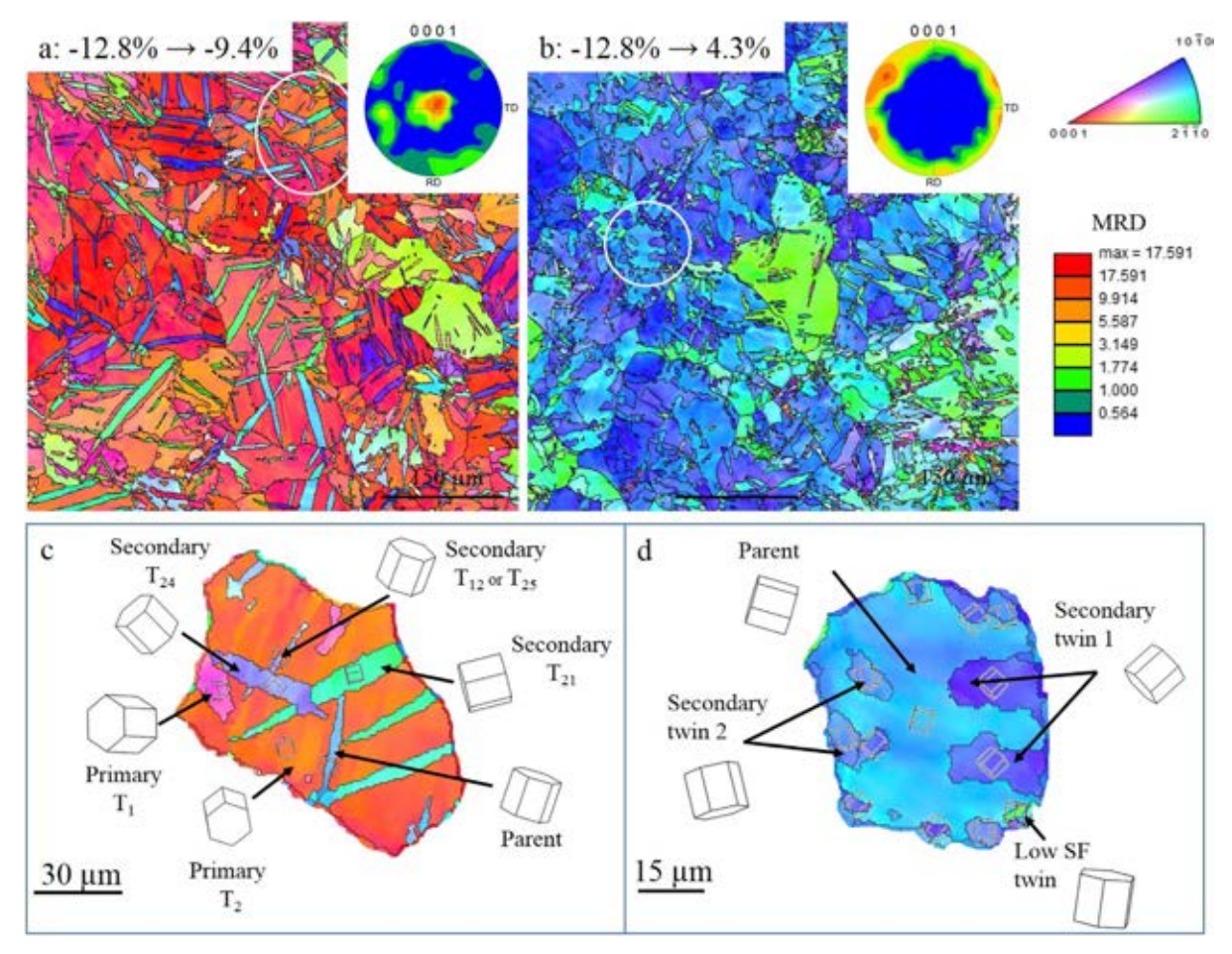


Fig. 5. EBSD inverse pole figure maps and pole figures for the (0001) plane for the -12.8% pre-strain path tensioned to (a) -9.4% strain and (b) 4.3% strain. (c) A grain marked in (a) that depicts both detwinning and new secondary twinning as results of the tensile loading. (d) A grain marked in (b) displays the sub-grains that are formed from secondary tension twinning and the low SF twins at tensile failure. (For interpretation of the references to color in this figure legend, the reader is referred to the web version of this article.)

4. Further Discussions

At -7.3% pre-strain, twinning does not exhaust the matrix. However at -12.8% pre-strain, twinning is exhausted in most grains. With subsequent tensile loading following pre-compression, detwinning and secondary tension-tension twinning occur simultaneously. With an identical strain applied after the pre-compression, the resulting microstructure is dependent on the amount of pre-strain in compression. At point A in Fig. 2 for -7.3% pre-strain, Fig. 4a and c show that the originally twinned material has been partially detwinned to the original orientation, and only one secondary twin variant is nucleated within the primary twin. At point C in Fig. 2 for -12.8% pre-strain, Fig. 5a and c reveal significant amount of secondary tension twins while detwinning is not prevalent.

The different twinning phenomena observed in the two pre-strain cases are related to the state of the primary twin upon the start of the reversed loading. First, comparing Fig. 5a with Fig. 4a, fewer amount of detwinned primary twins in the -12.8% pre-strain case than the -7.3% case signifies an increased resistance of detwinning due to the larger pre-compression. Additionally, it was observed that the formation of secondary tension twins under tension usually occurs within the nearly prismatic $\{10\overline{1}0\}$ parent grains. Based on a simple Schmid factor analysis, these grains are more easily twinned than the *a*-axis $\{2\overline{1}10\}$ grains under compression. As a result, the nearly $\{10\overline{1}0\}$ grains are more likely to be completely twinned even in the -7.3% pre-strain specimens. Therefore, based on the observations made from Figs. 4c and 5c, the amount of secondary twin variants activated in a particular grain is related to the extent of primary twinning activated under compression.

This also explains the presence of secondary twinning in the nearly $\{10\overline{1}0\}$ grains in the two pre-strain cases since the prismatic orientation favors tension twinning under compression.

Detwinning is dependent on the initial primary twinning. It was reported that detwinning has a lower activation stress than that of twinning due to nucleation [39]. This would indicate that the grains incompletely twinned at -7.3% pre-strain would be easier to detwin than to initiate secondary twinning. However, in the -12.8% pre-strain case where most grains have completely twinned, detwinning is more difficult to activate, most likely due to the formation of twin-twin boundaries associated with twin-twin interactions [13]. The exhausted primary twin formed in compression acts like a new or reoriented grain, wherein detwinning involves twin nucleation. The complicated stress state resulted from exhausted primary twins and dislocations allow for the increased amount of secondary twin variants as shown in Fig. 5c.

When the pre-compression strain exceeds a certain value, nucleation and growth of the secondary twins may halt and only detwinning occurs. Fragmented residual $\langle 10\bar{1}2\rangle$ - $\langle 10\bar{1}2\rangle$ double twins are observed to be surrounded by the fully detwinned parent material (Figs. 4d and 5d). Some of these fragments are double twins but appear as sub-grains. These double twins are usually isolated within a grain and do not interact with the grain boundaries. Based on these observations, the process of the secondary twinning and detwinning during reversed tension after pre-compression is rationalized as follows (Fig. 6). Twins (designated "T" in Fig. 6) with large SFs nucleate within the parent grain (designated "M" in Fig. 6) and grow during the pre-compression phase (Fig. 6a). With increasing compressive strain, the neighboring twin boundaries coalesce, forming low angle boundaries if the

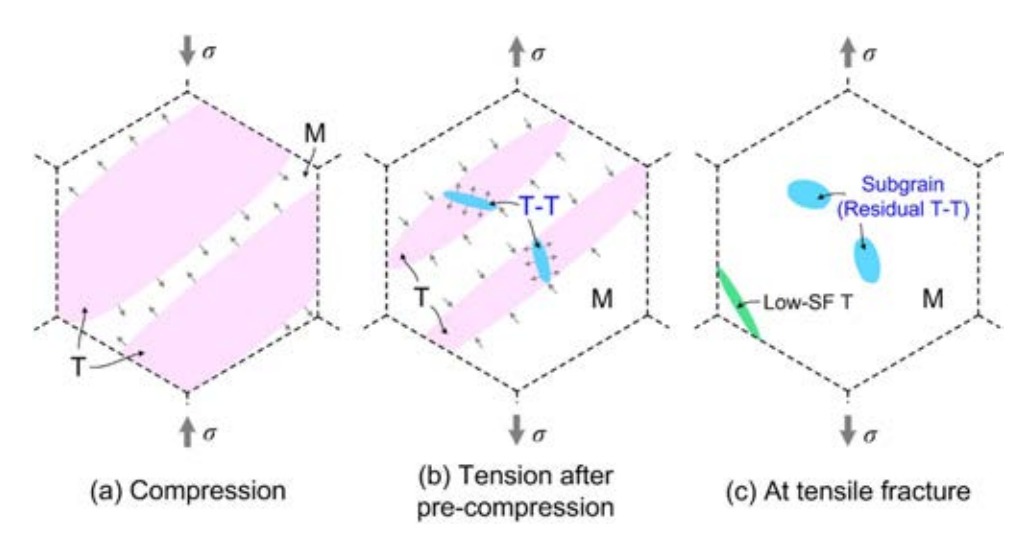


Fig. 6. Schematic showing the formation of subgrains due to secondary tension twinning during the tension loading after pre-compression. (For interpretation of the references to color in this figure, the reader is referred to the web version of this article.)

neighboring twins do not belong to the same variant or co-zone pair. When the loading direction is reversed to tension (Fig. 6b), detwinning of the previously developed primary twins occurs. Under reversed tension, the crystal orientation of the primary twin favors the activation of a secondary tension twin. As a result, secondary twinning is nucleated at primary twin boundaries ("blue" T-T twins in Fig. 6b). With further tensile loading, growth of secondary twins is possible but is restricted due to the constraints imposed by the sustainable detwinning of the primary twins. The competition between detwinning of the primary twins and growth of secondary twins results in the observed irregular shaped secondary twins. At tensile fracture (Fig. 6c), a majority of the twinned domain during pre-compression is detwinned. Secondary twin fragments, either isolated with a grain or connected to grain boundaries, remain inside the grain and form the observed subgrains. The boundaries of sub-grains have a specific misorientation property, which is possibly one of the three misorientation relationships of twin-twin interaction pairs [13].

The sub-grains resulted from the reserved tension of the pre-compressed specimens may play a critical role in strengthening materials. Fig. 7 shows the microstructures of the extruded pure Mg after fracture with three different loading conditions: monotonic tension (up to 7% strain), tension after -7.3% pre-compression, and tension after -12.8% compression (refer to Fig. 2 for the loading conditions). Low SF twins are observed in all the three fractured specimens. The major difference among the three cases lies in the sub-grain development. No sub-grains are found in the monotonically tensioned specimen (Fig. 7a) due to a lack of secondary tension twins. On the other hand, sub-grains are identified in the pre-compressed specimens, and the amount of sub-grains is

proportional to the amount of compressive pre-strain. It can be observed from the stress-strain curves shown in Fig. 2 that there is a noticeable increase in tensile fracture strength with increasing pre-compressive strain: an increase from 164 MPa for monotonic tension (no pre-compression) to 247 MPa for the -7.3% pre-strained specimen and to 264 MPa for the -12.8% pre-strain specimen. The observation supports the hypothesis that the sub-grains resulted from secondary twinning has an obvious effect on grain refinement and material's strength.

5. Conclusions

The following conclusions can be drawn from the observations and analysis of the microstructural and textural evolution of extruded pure polycrystalline Mg under reversed tensile loading after pre-compression:

- 1. The amount of twin variants activated under compression along the extrusion direction is dependent on the orientation of the grains. Grains close to the prismatic $\{10\overline{1}0\}$ orientation will contain up to one co-zone variant pair of similar Schmid factor. Alternatively, grains close to the a-axis $\{2\overline{1}10\}$ orientation can have multiple twin variants activated up to two sets of co-zone variant pairs of similar Schmid factor.
- 2. A combined deformation process of low-SF twinning, secondary twinning, and detwinning occurs as a result of the tensile loading after the grains have been severely twinned in compression. Under the reversed tension subsequent to large pre-compression, nucleation and growth of secondary tension twin are observed concurrent to detwining of primary twins.

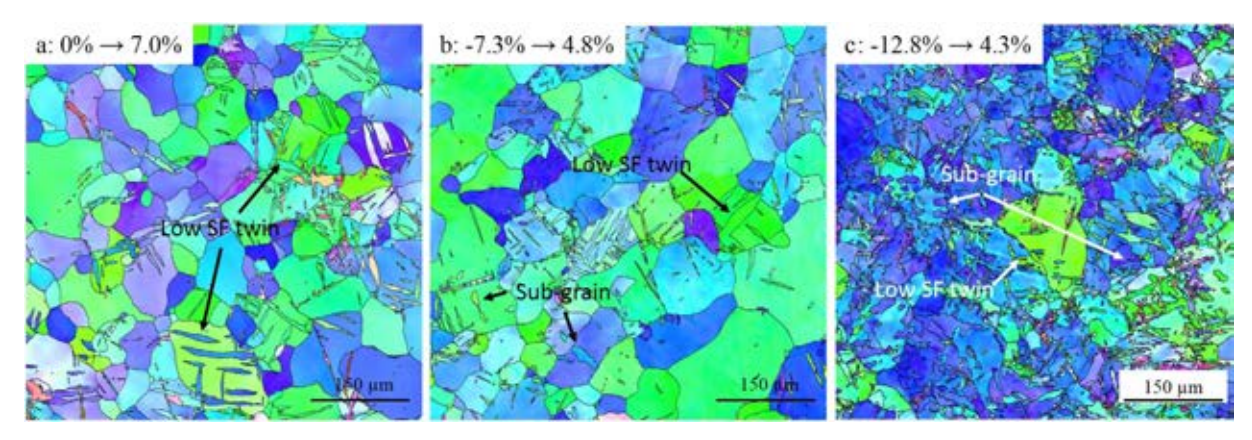


Fig. 7. EBSD IPF maps for fractured specimens with three loading paths (a) monotonic tension up to 7.0% strain, (b) tension after -7.3% pre-strain, and (c) tension after -12.8% pre-strain.

3. After -7.3% compression strain, one secondary twin variant is observed during subsequent tension. At least two secondary twin variants are commonly found in the -12.8% pre-strain specimens. The secondary twins form residual sub-grains within the detwinned grains, which leads to increased tensile strength.

Acknowledgements

The authors acknowledge supports from the US National Science Foundation (NSF) (CMMI-1462885 and CMMI-1661686).

References

- [1] M.H. Yoo, Slip, twinning, and fracture in hexagonal close-packed metals, Metall. Mater. Trans. A 12 (3) (1981) 409–418.
- [2] S.R. Agnew, P. Mehrotra, T.M. Lillo, G.M. Stoica, P.K. Liaw, Crystallographic texture evolution of three wrought magnesium alloys during equal channel angular extrusion, Mater. Sci. Eng. A 408 (1-2) (2005) 72-78.
- D.W. Brown, S.R. Agnew, M.A.M. Bourke, T.M. Holden, S.C. Vogel, S.N. Tomé, Internal strain and texture evolution during deformation twinning in magnesium, Mater. Sci. Eng. A 399 (2005) 1-12.
- M. Barnett, Twinning and the ductility of magnesium alloys Part II. "Contraction" twins, Mater. Sci. Eng. A 464 (1–2) (2007) 8–16.

 L. Meng, P. Yang, Q. Xie, W. Mao, Analyses on compression twins in magnesium,
- Mater, Trans. 49 (4) (2008) 710-714.
- P. Cizek, M.R. Barnett, Characteristics of the contraction twins formed close to the fracture surface in Mg-3Al-1Zn alloy deformed in tension, Scr. Mater. 59 (9) (2008)
- F. Mokdad, D.L. Chen, D.Y. Li, Single and double twin nucleation, growth, and interaction in an extruded magnesium alloy, Mater. Des. 119 (2017) 376-396.
- É. Martin, L. Capolungo, L. Jiang, J.J. Jonas, Variant selection during secondary twining in Mg-3%Al, Acta Mater, 58 (2010) 1970-3983.
- D. Ando, J. Koike, Y. Sutou, Relationship between deformation twinning and surface step formation in AZ31 magnesium alloys, Acta Mater. 58 (2010) 4316-6324.
- [10] I.J. Beyerlein, J. Wang, M.R. Barnett, C.N. Tomé, Double twinning mechanisms in magnesium alloys via dissociation of lattice dislocations, Proc. R. Soc. A 468 (2012) 1496-1520
- [11] A. Jäger, A. Ostapovets, P. Molnár, P. Lejček, {10-12}-{10-12} Double twinning in magnesium, Philos. Mag. Lett. 91 (2001) 537-544.
- [12] Y. Xin, X. Zhou, Q. Liu, Suppressing the tension-compression yield asymmetry of Mg alloy by hybrid extension twins structure, Mater. Sci. Eng. A 567 (2013) 9-13.
- Q. Yu, J. Wang, Y. Jiang, R.J. McCabe, Li Nan, C.N. Tomé, Twin-twin interactions in magnesium, Acta Mater. 77 (2014) 28-42.
- [14] Y. Xin, X. Zhou, L. Lv, Q. Liu, The influence of secondary twin on the detwinning deformation of a primary twin in Mg-3Al-1Zn alloy, Mater. Sci. Eng. A 606 (2014) 81_91
- [15] S. Mu, J.J. Jonas, G. Gottstein, Variant selection of primary, secondary, and tertiary twins in a deformed Mg alloy, Acta Mater. 60 (2012) 2043-2053.
- [16] Q. Yu, Y. Jiang, J. Wang, Tension-compression-tension tertiary twins in coarsegrained polycrystalline pure magnesium at room temperature, Philos. Mag. Lett. 95 (2015) 194-201.
- [17] H. Watanabe, A. Takara, H. Somekawa, T. Mukai, K. Higashi, Effect of texture on tensile properties at elevated temperatures in an AZ31 magnesium alloy, Scr. Mater. 52 (2005) 449–454.
- [18] S.B. Yi, C.H.J. Davies, H.G. Brokmeier, R.E. Bolmaro, K.U. Kainer, J. Homeyer, Deformation and texture evolution in AZ31 magnesium alloy during uniaxial loading, Acta Mater. 54 (2006) 549-562.
- J. Jiang, A. Godfrey, W. Liu, Q. Liu, Microtexture evolution via deformation twinning and slip during compression of magnesium alloy AZ31, Mater. Sci. Eng. A 483-484 (2008) 576-579.
- [20] J. Jiang, A. Godfrey, W. Liu, Q. Liu, Identification and analysis of twinning variants during compression of a Mg-Al-Zn alloy, Scr. Mater. 58 (2008) 122-125.
- Y. Chino, K. Kimura, M. Hakamada, M. Mabuchi, Mechanical anisotropy due to twinning in an extruded AZ31 Mg alloy, Mater. Sci. Eng. A 485 (2008) 311-317.
- [22] S.-G. Hong, S.H. Park, C.S. Lee, Role of {10-12} twinning characteristics in the deformation behavior of a polycrystalline magnesium alloy, Acta Mater. 58 (2010) 5873-5885.
- Y. Xin, M. Wang, Z. Zeng, M. Nie, Q. Liu, Strengthening and toughening of magnesium alloy by {10-12} extension twins, Scr. Mater. 66 (2012) 25-28.
- Q. Ma, H. El Kadiri, A.L. Oppedal, J.C. Baird, B. Li, M.F. Horstemeyer, S.C. Vogel, Twinning effects in a rod-textured AM30 Magnesium alloy, Int. J. Plast. 29 (2012)
- [25] J. Sun, L. Jin, S. Dong, Z. Zhang, J. Dong, Asymmetry strain hardening behavior in Mg-3%Al-1%Zn and Mg-8%Gd-3%Y alloy tubes, Mater. Lett. 107 (2013) 197-201.
- [26] D. Sarker, J. Friedman, D.L. Chen, Twin growth and texture evolution in an extruded AM30 magnesium alloy during compression, J. Mater. Sci. Technol. 30 (9) (2014) 884-887.

- [27] D. Sarker, J. Friedman, D.L. Chen, De-twinning and texture change in an extruded AM30 magnesium alloy during compression along normal direction, J. Mater. Sci. Technol. 21 (2015) 264-268.
- L. Wu, A. Jain, D.W. Brown, G.M. Stoica, S.R. Agnew, B. Clausen, et al., Twinningdetwinning behavior during the strain-controlled low-cycle fatigue testing of a wrought magnesium alloy, ZK60A, Acta Mater. 56 (2008) 688-695.
- [29] L. Wu, S.R. Agnew, D.W. Brown, G.M. Stoica, B. Clausen, A. Jain, et al., Internal stress relaxation and load redistribution during the twinning-detwinning-dominated cyclic deformation of a wrought magnesium alloy, ZK60A, Acta Mater. 56 (2008)
- [30] L. Wu, S.R. Agnew, Y. Ren, D.W. Brown, B. Clausen, G.M. Stoica, et al., The effects of texture and extension twinning on the low-cycle fatigue behavior of a rolled magnesium alloy, AZ31B, Mater. Sci. Eng. A 57 (2010) 7057-5067.
- [31] S.H. Park, S.-G. Hong, B.H. Lee, W. Bang, C.S. Lee, Low-cycle fatigue characteristics of rolled Mg-3Al-1Zn alloy, Int. J. Fatigue 32 (2010) 1835-1842.
- S.H. Park, S.-G. Hong, W. Bang, C.S. Lee, Effect of anisotropy on the low-cycle fatigue behavior of rolled AZ31 magnesium alloy, Mater. Sci. Eng. A 527 (2010)
- [33] M. Huppmann, M. Lentz, S. Chedid, W. Reimers, Analyses of deformation twinning in the extruded magnesium alloy AZ31 after compressive and cyclic loading, J. Mater. Sci. 46 (2011) 938-950.
- [34] O. Yu, J. Zhang, Y. Jiang, Direct observation of twinning-detwinning-retwinning on magnesium single crystal subjected to strain-controlled cyclic tension-compression in [0001] direction, Philos. Mag. Lett. 91 (12) (2011) 757-765.
- [35] Q. Yu, J. Zhang, Y. Jiang, Q. Li, An experimental study on cyclic deformation and fatigue of extruded ZK60 magnesium alloy, Int. J. Fatigue 36 (1) (2012) 47-58.
- [36] S. Dong, O. Yu, Y. Jiang, J. Dong, F. Wang, W. Ding, Electron backscatter diffraction observations of twinning-detwinning evolution in a magnesium alloy subjected to large strain amplitude cyclic loading, Mater. Des. 65 (2015) 762-765.
- G. Proust, C.N. Tomé, A. Jain, S.R. Agnew, Modeling the effect of twinning and detwinning during strain-path changes of magnesium alloy AZ31, Int. J. Plast. 25 (2009) 861–880.
- [38] L. Wang, G. Huang, Q. Quan, P. Bassani, E. Mostaed, M. Vedani, F. Pan, The effect of twinning and detwinning on the mechanical property of AZ31 extruded magnesium alloy during strain-path changes, Mater. Des. 63 (2014) 177-184.
- X.Y. Lou, M. Li, R.K. Boger, S.R. Agnew, R.H. Wagoner, Hardening evolution of AZ31B Mg sheet, Int. J. Plast. 23 (2007) 44-86.
- [40] J. He, T. Liu, Y. Zhang, J. Tan, Twin characteristics and flow stress evolution in extruded magnesium alloy az31 subjected to multiple loads, J. Alloys Compd. 578 (2013) 536-542.
- [41] J. He, T. Liu, S. Xu, Y. Zhang, The effects of compressive pre-deformation on yield asymmetry in hot-extruded Mg-3Al-1Zn alloy, Mater. Sci. Eng. A 579 (2013) 1-8.
- [42] D. Sarker, D.L. Chen, Dependence of compressive deformation on pre-strain and loading direction in an extruded magnesium alloy: texture, twinning and de-twinning, Mater. Sci. Eng. A 596 (2014) 134-144.
- [43] Y. Xin, J. Jiang, A. Chapuis, M. Wang, Q. Liu, Plastic deformation behavior of AZ31 magnesium alloy under multiple passes cross compression, Mater. Sci. Eng. A 532 (2012) 50-57.
- B. Song, R. Xin, Y. Liang, G. Chen, Q. Liu, Twinning characteristic and variant selection in compression of a pre-side-rolled Mg alloy sheet, Mater. Sci. Eng. A 614 (2014) 106-115.
- [45] D. Sarker, J. Friedman, D.L. Chen, Influence of pre-strain on de-twinning activity in an extruded AM30 magnesium alloy, Mater. Sci. Eng. A 605 (2014) 73-79.
- Z. Long, T. Liu, Y. Wu, Y. Zhang, Improving the anisotropy of rolled Mg-3Al-1Zn alloy by pre-strain and annealing, Mater. Sci. Eng. A 616 (2014) 240-245.
- [47] D. Sarker, J. Friedman, D.L. Chen, Influence of pre-deformation and subsequent annealing on strain hardening and anisotropy of AM30 magnesium alloy, J. Alloys Compd. 611 (2014) 341-350.
- [48] A. Chapuis, Y. Xin, X. Zhou, Q. Liu, {10-12} Twin variants selection mechanisms during twinning, re-twinning and detwinning, Mater. Sci. Eng. A 612 (2014) 431-439
- [49] B. Song, R. Xin, X. Zheng, G. Chen, Q. Liu, Activation of multiple twins by pretension and compression to enhance the strength of Mg-3Al-1Zn alloy plates, Mater. Sci. Eng. A 621 (2015) 100-104.
- L. Wang, G. Huang, Q. Quan, P. Bassani, E. Mostaed, M. Vedani, F. Pan, The effect of twinning and detwinning on the mechanical property of AZ31 extruded magnesium alloy during strain-path changes, Mater. Des. 63 (2014) 177-184.
- C. Lou, X. Zhang, R. Wang, Q. Liu, Mechanical behavior and microstructural characteristics of magnesium alloy containing {10-12} twin lamellar structure, J. Mater. Res. 28 (5) (2012) 733-739.
- [52] S.-F. Chen, L. Zheng, S.-H. Zhang, H.-W. Song, M. Cheng, Deformation mechanism of AZ31B magnesium alloy under different loading paths, Acta Metall. Sin. 28 (12) (2015) 1426–1434 (English Letters).
- [53] L. Wang, G. Huang, Q. Quan, P. Bassani, E. Mostaed, M. Vedani, F. Pan, The effect of twinning and detwinning on the mechanical property of AZ31 extruded magnesium alloy during strain-path changes, Mater. Des. 63 (2014) 177-184.
- K.D. Molodov, T. Al-Samman, D.A. Molodov, G. Gottstein, On the role of anomalous twinning in the plasticity of magnesium, Acta Mater. 103 (2016) 711-723.
- [55] D. Liu, R. Xin, Y. Hongni, Z. Liu, X. Zheng, Q. Liu, Comparative examinations on the activity and variant selection of twinning during tension and compression of magnesium alloys, Mater. Sci. Eng. A 658 (2016) 229-237.